Neoplasia 35 (2023) 100862

Contents lists available at ScienceDirect

Neoplasia

journal homepage: www.elsevier.com/locate/neo

Original Research

Targeting Na-H exchanger 1 overcomes nuclear factor kappa B-mediated tumor resistance to radiotherapy

Arang Son[a,1], Seoyeong Kang[b,1], Suha Choi[a], Sung-Won Shin[a], Yeeun Kim[a], Wankyu Kim[b,*], Changhoon Choi[a,*]

[a] Department of Radiation Oncology, Samsung Medical Center, Seoul 06351, South Korea
[b] Department of Life Sciences, Ewha Womans University, Seoul 03760, South Korea

ARTICLE INFO

Keywords:
Radiation therapy
Acquired radioresistance
Na-H exchanger 1
NF-κB

ABSTRACT

Intrinsic or acquired radioresistance often limits the efficacy of radiation therapy (RT), thereby leading to local control failure. Cancerous cells have abnormal pH dynamics due to high metabolic demands, but it is unclear how pH dynamics contribute to radioresistance. In this study, we investigated the role of Na-H exchange 1 (NHE1), the major intracellular pH (pH_i) regulator, in RT response. We observed that RT increased NHE1 expression and modulated pH_i in MDA-MB-231 human breast cancer cells. When combined with RT, pharmacological NHE1 inhibition by 5-(N-Ethyl-N-isopropyl)amiloride (EIPA) reduced pH_i and clonogenic survival. EIPA attenuated radiation-damaged DNA repair, increasing G2/M cell cycle arrest. The combination of EIPA and RT increased apoptotic cell death while decreasing phosphorylation of NF-κB p65. Similarly, the knockdown of NHE1 increased radiosensitivity with lower pH_i and increased apoptosis. Consistent with in vitro data, the EIPA plus RT inhibited the growth of MDA-MB-231 xenograft tumors in mice to a greater extent than either EIPA or RT alone. EIPA abrogated the RT-induced increase in NHE1 and phospho-NF-κB p65 expression in tumor tissues. Such coincidence of increased NHE1 level, pH_i, and NF-κB activation was also found in radioresistant MDA-MB-231 cells, which were reversed by EIPA treatment. Bioinformatics analysis of RNA sequencing data revealed that inhibiting NHE1 reversed three core gene networks that were up-regulated in radioresistant cells and correlated with high NHE1 expression in patient samples: NF-κB, senescence, and extracellular matrix. Taken together, our findings suggest that NHE1 contributes to RT resistance via NF-κB-mediated signaling networks, and NHE1 may be a promising target for improving RT outcomes.

Introduction

Emerging data suggest that aberrant pH dynamics is one of the characteristics that cancer cells acquire adaptively [1,2]. Cancerous cells have a reversed pH gradient, with a higher intracellular pH (pH_i) of ≥ 7.2 and a lower extracellular pH (pH_e) of 6.7 – 7.1, compared to normal cells, which have lower pH_i and higher pH_e. This is primarily due to increased proliferative and metabolic activities of cancer cells when compared to normal cells. Indeed, various net acid extruders, including H^+-ATPases, the Na^+-H^+ exchanger NHE1, and the monocarboxylate-H^+ efflux cotransporters MCT1 and MCT4 are upregulated or activated in cancerous tissues to maintain pH homeostasis, and various therapeutic strategies to exploit this pH dysregulation have been tested [3].

Cancer cells benefit from the reversed pH gradient in proliferation, survival, metabolism, migration, and metastasis. Increased pH_i promotes proliferation as a permissive signal for growth factor-stimulated cell cycle progression, particularly the G2/M transition [4]. It also allows cancer cells to avoid apoptosis [5,6]. Aerobic glycolysis, also known as the Warburg effect, is an essential metabolic feature of cancer cells, and pH sensors like phosphofructokinase-1 are involved in pH_i-regulated metabolism [7]. Another example of pH-regulated cancer cell behavior is directed cell migration. Migrating cells remodel actin filaments and cell-substrate adhesion, which is regulated by intracellular pH sensors such as focal adhesion kinase [8]. Decreased pH_e not only causes melanoma cells to migrate faster by modulating integrin-extracellular matrix attachments [9] but it also is required for invadopodium maturation and matrix metalloproteinase activation, which facilitates invasion and metastasis [10].

Among the many pH regulators, NHE1 (*SLC9A1*), a member of the solute carrier family 9, plays a critical role in pH_i maintenance. NHE1 expression or activity is elevated in various types of cancers, including gastric cancer [11], ovarian cancer [12], and glioma tissues [13] and is

* Corresponding authors.
E-mail address: chchoi93@gmail.com (C. Choi).
[1] These authors contributed equally.

https://doi.org/10.1016/j.neo.2022.100862
Received 10 October 2022; Received in revised form 30 November 2022; Accepted 30 November 2022

associated with poor prognosis. Previous research has shown that NHE1-deficient human bladder carcinoma cells and triple-negative breast cancer cells grow poorly in immune-compromised mice, implying that NHE1 is required for tumor growth [14,15]. Pharmacological inhibition of NHE1 demonstrates anti-cancer efficacy in pancreatic cancer [16], and fibrosarcoma [17] mouse xenograft models. Furthermore, NHE1 inhibition re-sensitizes drug-resistant cancer [15,18] and works synergistically with targeted therapies like erlotinib [19] and immunotherapy [20].

Radiation therapy (RT) is one of the most effective treatment modalities for solid cancer, but it is limited by intrinsic or acquired radioresistance. Several preclinical studies have been conducted to investigate the roles of net acid excluders in RT response. Interrupting lactate transport by inhibiting either MCT1 or mitochondrial pyruvate carrier increased radiosensitivity in small cell lung cancer and cervical cancer xenografts [21,22]. Carbonic anhydrase IX (CA9), which contributes to acidic pH_e, is linked to tumor hypoxia and radioresistance. Its inhibition makes breast cancer, renal cell carcinoma, and colon carcinoma sensitive to RT [23,24]. NHE1 inhibition diminishes the pH_i-regulating capacity of fibroblast and cancer cells, increasing radiosensitivity [24], but the underlying mechanisms remain unknown. The goal of this study was to investigate the mechanism of NHE1-regulated radioresistance.

Materials and methods

Cell culture

MDA-MB-231 human triple-negative breast cancer (TNBC) cell line was obtained from the American Type Culture Collection (ATCC, Manassas, VA, USA), and AsPC-1 human pancreatic cancer cell lines were obtained from Korean Cell Line Bank (Seoul National University, Seoul, Korea). MDA-MB-231 and AsPC-1 cells were cultured in Dulbecco's Modified Eagle Medium (DMEM) supplemented with 10 % fetal bovine serum (FBS), 1 × antibiotic-antimycotic solution (AA, Thermo Fisher Scientific, Waltham, MA, USA) and 25 mM HEPES (Gibco, Carlsbad, CA, USA). The radioresistant MDA-MB-231 cell line (MDA-MB-231RR) was established by exposing the parental MDA-MB-231 cell line to cumulative doses (total of 40 Gy) of radiation. Initially, a daily dose of 2 Gy was delivered to the cells over 5 days for 2 weeks. After resting for 2 weeks, the cells were collected and plated at low density. The cells were irradiated with an additional daily dose of 5 Gy twice a week for 2 weeks and the surviving cells were pooled. Acquired radioresistance was determined by clonogenic survival assay. Cultures were kept in a humidified atmosphere of 95 % air/5 % CO_2 at 37°C.

Reagents and antibodies

5-(N-Ethyl-N-isopropyl)amiloride (EIPA) was purchased from Tocris Bioscience (Bristol, UK). Anti-phospho-H2AX (Ser139), anti-phospho-ATR (Ser428), anti-phospho-Chk2 (Thr68), anti-NF-κB p65, and anti-cleaved PARP antibodies were purchased from Cell Signaling Technology (Danvers, MA, USA). Anti-β-actin antibodies were purchased from Sigma Aldrich (St. Louis, MO, USA). Anti-NHE1 and anti-MCT1 antibodies were purchased from Santa Cruz Biotechnology (Santa Cruz, CA, USA). Anti-phospho-NF-κB p65(Ser529) antibodies were purchased from BD bioscience (Franklin, NJ, USA).

Cell viability assay

Cell viability was determined using a CCK-8 (Cell Counting Kit-8, Dojindo Laboratories, Kumamoto, Japan) assay. MDA-MB-231 and AsPC-1 cells were seeded into a 96-well plate at 1×10^4 cells/well and treated with various concentrations of EIPA. Cell viability was calculated as a percentage relative to the untreated control by measuring the absorbance at 450 nm with a SpectraMax i3 microplate reader (Molecular Devices, Sunnyvale, CA, USA).

Irradiation

A single-cell suspension of exponentially growing cells was seeded on cell dishes a day before irradiation. At a source surface distance of 100 cm and a field size of 30 × 30 cm, the dishes were placed beneath a 2 cm thick solid water phantom. X-ray beams were delivered at a dose rate of 3.96 Gy per min using a Varian Clinac 6EX linear accelerator (Varian Medical Systems, Palo Alto, CA, USA). The absolute X-ray dose was verified to a 1 % accuracy in accordance with TG-51.

Clonogenic assay

The clonogenic survival assay was used to determine radiosensitivity. Cells were incubated for 7-14 days after irradiation. Surviving colonies with more than 50 cells were counted after being stained with 0.5 % crystal violet. The survival fraction was calculated as a ratio of the plating efficiency (number of surviving colonies to number of plated cells) of the irradiated cells to mock-irradiated cells. The dose-response curves were drawn using GraphPad Prism 9.3.1 (GraphPad Software, La Jolla, CA, USA) and were fitted by a linear-quadratic equation [$SF = \exp(-\alpha D - \beta D^2)$; SF, survival fraction; D, absorbed dose]. The dose enhancement factor (DEF) of EIPA is the ratio of the radiation doses resulting in 10% survival comparing control samples.

Bioluminescence assay

Caspase-Glo 3/7 reagent assay (Promega, Madison, WI, USA) was performed according to the manufacturer's instructions. Briefly, MDA-MB-231 cells were seeded at 1×10^4 cells/well into a clear bottom white 96-well plate, then incubated with 20 μM EIPA, followed by IR. After 48 h, 100 μL of Caspase-Glo 3/7 reagent was added, and luminescence was measured with a SpectraMax i3 microplate reader (Molecular Devices, Sunnyvale, CA, USA).

For measuring NF-κB activity, cells were transfected with an NF-κB promoter-luciferase plasmid (pGL4.32[luc2P/NF-κB-RE/Hygro], Promega) and Renilla luciferase plasmid (pRL-TK, Promega) using Lipofectamine 3000 (Thermo Fisher Scientific) according to the manufacturer's instructions. EIPA was applied to transfected cells for 24 h. Luciferase activity was measured using a Dual-Glo luciferase assay system (Promega).

Intracellular pH measurement

Intracellular pH was determined by using the pHrodo Green AM intracellular pH indicator (Thermo Fisher Scientific) according to the manufacturer's instructions. Briefly, cells were seeded at 2×10^4 cells/well into a clear bottom black 96-well plate. Cells were washed with Live Cell Imaging Solution (LCIS) and stained for 30 min with the pHrodo AM Ester staining solution. The fluorescence intensity was determined using a SpectraMax i3 microplate reader with excitation/emission wavelengths of 509/533 nm. A pH_i titration curve was obtained by incubating with pH_i calibration buffers containing nigericin and valinomycin (pH 5.5, 6.5, and 7.5).

Small interfering RNA (siRNA) transfection

Cells (1×10^6) were transfected with 10 nM siRNA designed for NHE1 knockdown (sc-42650, Santa Cruz Biotechnology) by using Lipofectamine RNAi MAX reagent (Thermo Fisher Scientific, Waltham, MA, USA), according to the manufacturer's instructions. Non-targeting siRNA (sc-37007) was used for control experiments.

Western blot analysis

Cells were lysed in modified RIPA buffer (20 mM Tris (pH 8.0), 137 mM NaCl, 10 % glycerol, 1 % Nonidet P-40, 10 mM EDTA, 100 mM

NaF, 1 mM phenylmethylsulfonyl fluoride and 10 mg/mLleupeptin), and the pellet was removed after 15 min of centrifugation at 13,000 rpm. Protein concentration was determined using the Bio-Rad protein assay reagent (Bio-Rad, Richmond, CA, USA) according to the manufacturer's instructions. Sodium dodecyl sulfate-polyacrylamide gel electrophoresis (SDS-PAGE) was carried out on equal amounts of protein. Proteins were separated and transferred to nitrocellulose membranes (Bio-Rad); blots were blocked overnight with 5 % skimmed milk in PBS at 4°C before being treated with primary antibodies overnight. Protein bands were detected using the Amersham enhanced chemiluminescence detection reagents (GE Healthcare, Piscataway, NJ, USA).

Flow cytometry

For apoptosis detection, harvested cells were stained with annexin V-FITC (BD Pharmingen, San Diego, CA, USA), and 2 μg/mL propidium iodide (PI) was added to the annexin V binding buffer (10 mM HEPES, pH 7.4, 140 mM NaCl, 2.5 mM $CaCl_2$) in the dark for 15 min at 37°C. The number of apoptotic cells was quantified using a BD FACSVerse flow cytometer and the BD FACSuite software. For the cell cycle analysis, harvested cells were fixed with pre-chilled 70% ethanol and were incubated with 1 mg/mL RNase and 50 μg/mL PI in the dark for 30 min at 37°C.

Immunofluorescence

Cells cultured on cover glasses were fixed with 4% formaldehyde and permeabilized with 0.01% Triton X-100. After 30 min of blocking with 2% FBS, cells were incubated with primary γ-H2AX antibody for 1 h, followed by DAPI (Sigma-Aldrich) and Alexa Fluor-488-conjugated secondary antibody (Life Technologies) for 30 min. After that, the cells were washed, mounted with a fluorescent mounting medium (Dako, Carpinteria, CA, USA), and examined under a fluorescence microscope (Zeiss Observer D1; Carl Zeiss Co., Ltd. Carpinteria, CA, USA)

Animal models

All animal procedures were conducted in accordance with appropriate regulatory standards under a protocol (ID: 20200909002; approval date: 2020-09-01) approved by the Institutional Animal Care and Use Committee (IACUC) of the Samsung Biomedical Research Institute (SBRI). The SBRI is an accredited facility of the Association for Assessment and Accreditation of Laboratory Animal Care International (AAALAC International) and abides by the Institute of Laboratory Animal Resources (ILAR) guidelines.

For the MDA-MB-231 tumor model, 6–7-week-old female BALB/c mice were purchased from Orient Bio (Gapyeong, Korea). Cells (5×10^6 cells/50 μL PBS) were injected subcutaneously into the right hind leg. Tumor volumes were measured every 3 days with calipers and calculated according to the following formula: volume = width^2 × length ÷ 2. When the mean tumor volume reached 80–120 mm^3, mice were randomly assigned to one of four groups. EIPA (12 mg/kg) was given intraperitoneally three times a week for the first two weeks, then twice a week for the next two weeks. The tumor was irradiated with 6 Gy X-ray to the right hind leg two hours after drug treatment. The mice were intraperitoneally anesthetized with 30 mg/kg of Zoletil (Virbac, Carros, France) and 10 mg/kg of Rompun (Bayer, Leverkusen, Germany).

TUNEL and immunohistochemistry

The terminal deoxynucleotidyl transferase dUTP nick end labeling (TUNEL) assay was used to detect apoptosis in tumor tissues. Slices of paraffin-embedded tissues were deparaffinized in water and placed in 3% H_2O_2 at room temperature for 10 min. The ApopTag® Peroxidase In Situ Apoptosis Detection Kit (Millipore) was used according to the manufacturer's instructions. TUNEL-positive cells were imaged and quantified using the imageScope software on an Aperio ScanScope AT instrument (Leica Biosystems, Buffalo Grove, IL, USA).

For immunohistochemistry, the paraffin-embedded tissue sections were deparaffinized three times in xylene for 15 min before being rehydrated. Immunostaining for NHE1 and phospho-NF-κB p65 was performed using the Bond-MaxTM polymer refine detection kit (Vision Biosystems, Melbourne, Australia). Antigen retrieval was performed in ER1 buffer at 97°C for 20 min. For 10 min, 3% H_2O_2 was used to inhibit endogenous peroxidase activity. The primary antibody incubation was performed for 15 min at room temperature.

Statistics

Statistical analysis was performed using GraphPad Prism 9.3.1. The statistical significance of differences among groups was calculated with one-way or two-way ANOVA with Tukey's multiple comparisons post-hoc test. All p-values < 0.05 were considered statistically significant.

RNA-sequencing and preprocessing

MDA-MB-231-RR cells were treated with 20 or 50 μM EIPA and harvested after 24 h. Total RNA was extracted using TRIzol reagent (Thermo Fisher Scientific). Transcriptome data was produced by Illumina NovaSeq 6000 and TruSeq Stranded mRNA library Kit. The reads were aligned to the GRCh38 reference genome using STAR (v2.7.1a) [25], and gene expression was quantified with RSEM (v1.3.1) [26]. Only protein-coding genes were used for subsequent analysis.

Differential expression analysis

Differential expression analysis was performed using DESeq2 [27]. For wild-type and radioresistance samples (WT versus RR group), analysis was performed by batch and the resulting differentially expressed genes (DEGs) were aggregated (fold change > 2, FDR < 0.01). For EIPA-treated samples (EIPA versus RR group), different thresholds were applied for each drug concentration (fold change > 1.5 and FDR < 0.3 for 20 μM, fold change > 2, and FDR < 0.01 for 50 μM). Pathway and transcription factor analysis were performed using a hypergeometric test. Gene sets were collected from MSigDB (v7.4) [28] and Harmonizome [29]. The gene network was constructed from STRING protein-protein interaction database [30] and visualized using Cytoscape [31]. The density of gene network was defined by the following formula:

$$Network\ density = \frac{E}{\frac{N(N-1)}{2}}$$

Where E represents the number of total edges in the network and N represents the number of nodes.

The cancer genome atlas (TCGA) data analysis

The expression data of BRCA patients in TCGA (http://cancergenome.nih.gov/) was downloaded from the NCI Genomic Data Commons (GDC) Data Portal [32] and the partial annotation data was from the GDC Legacy Archive.

The TNBC patients were selected by expression (FPKM) of ERBB2, ESR1, and PGR. The FPKM cut-off of triple genes was decided (ERBB2 < 30, ESR1 < 10, PGR < 10) based on 127 TNBC patients whose triple genes were annotated as Negative by Immunohistochemistry (IHC). Using these criteria, 239 out of 1222 BRCA patients were conservatively assumed as TNBC. These patients either received radiotherapy (RT, n = 123) or did not (noRT, n = 81).

Gene Set enrichment analysis (GSEA) [33] for each individual sample was performed using *fgsea* package [34] with geneset enriched in MDA-MB-231RR models. Samples were sorted by the sum of normalized enrichment scores (NES) and classified as NES-high and –low groups (100 each for TNBC, 60 for RT, and 40 for noRT). Comparison of NHE1

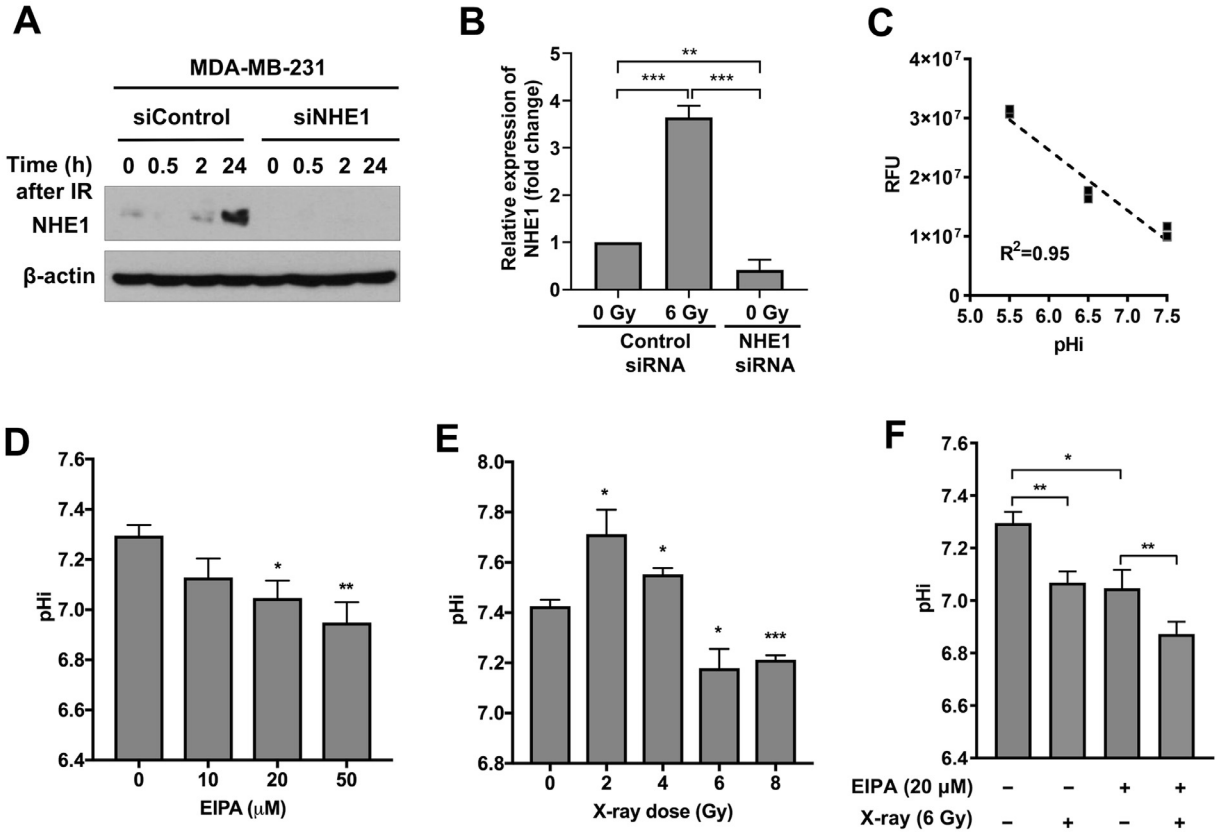

Fig. 1. Ionizing radiation increases the expression of the Na-H exchanger 1 (NHE1) and alters intracellular pH (pH_i). (A) Western blot analysis showed an increase in NHE1 expression following X-ray irradiation with 6 Gy. In MDA-MB-231 cells, samples were collected at the indicated times (h) after irradiation. β-actin was used as a loading control. (B) NHE1 expression quantification. (C) A pH_i titration curve with the fluorometric pHrodo Green probe. (D) EIPA, 5-(N-Ethyl-N-isopropyl)amiloride, a selective NHE1 inhibitor, decreased pH_i concentration-dependently. (E) Modulation of pH_i by ionizing radiation. (F) Combining EIPA and X-rays reduced pH_i even further in MDA-MB-231 cells. The data represent the mean ± SD (n = 3). * $p < 0.05$, ** $p < 0.01$, *** $p < 0.001$.

expression between groups was performed using the Wilcoxon test, and survival analysis was performed using the *survival* package, which estimates through the log-rank test.

Results

Pharmacological inhibition of NHE1 decreases steady-state intracellular pH in MDA-MB-231 cells

To determine the role of pH_i in radiation response, we first investigated how ionizing radiation affects NHE1, a key regulator of cellular pH homeostasis. Western blot analysis showed that the NHE1 level increased 3.6-fold 24 h post-irradiation (Fig. 1A and B). siRNA treatment confirmed the specificity of NHE1 immunoblotting. We then used a pH-sensitive fluorescence dye, pHrodo Green, to measure radiation-mediated changes in steady-state pH_i. A pH titration curve was created using three different pH calibration buffers, demonstrating linearity within a pH range of 5.5 to 7.5 (Fig. 1C). Treatment with an NHE1 inhibitor 5-(N-Ethyl-N-isopropyl)amiloride (EIPA) decreased pH_i in a concentration-dependent manner (Fig. 1D). Low-dose radiation, such as 2 Gy, increased pH_i from 7.4 to 7.7 (Fig. 1E). However, high-dose radiation above 6 Gy decreased pH_i (Fig. 1E), and its combination with EIPA decreased pH_i even more (Fig. 1F).

Pharmacological inhibition of NHE1 increases radiation sensitivity in MDA-MB-231 and AsPC-1 cells

EIPA treatment modestly decreased MDA-MB-231 and AsPC-1 cell viability in a dose-dependent manner at 48 h (Fig. 2A). We performed a clonogenic survival assay to see how inhibition of NHE1 affected radiosensitivity. Treatment with 5 μM EIPA significantly decreased the plating efficiency of MDA-MB-231 cells (from 52% to 35%, $p < 0.001$). Since only a few colonies grow at concentrations higher than 5 μM, we chose 5 μM for the clonogenic survival assay. Pre-treatment with EIPA significantly reduced clonogenic survival of MDA-MB-231 and AsPC-1 cells in response to irradiation (DEF_{10} = 1.43 and 1.20 for MDA-MB-231 and As-PC-1 cells, respectively; Fig. 2B), indicating that EIPA exerts a radiosensitizing effect. EIPA was also found to have a cytotoxic effect on breast and pancreatic cancer spheroids grown in 3D culture (Fig. S1A and B). EIPA inhibited the growth of MDA-MB-231 and AsPC-1 spheroids even more when combined with radiation (Fig. S1C).

To better understand how EIPA exerts a radiosensitizing effect, we investigated its impact on radiation-induced DNA damage response and cell cycle in MDA-MB-231 cells. We used 20 μM EIPA because it significantly reduced pH_i (Fig. 1D). Time-dependent analysis revealed that the expression of γ-H2AX, a DNA double-strand break (DSB) marker, increased 30 min after irradiation and decreased 24 h later (Fig. 2C). Radiation-induced expression of γ-H2AX and phospho-CHK2 was delayed by pre-treatment with 20 μM EIPA (Fig. 2C). Immunofluorescence revealed that the nuclei of cells co-treated with EIPA and radiation for 24 h had more foci of γ-H2AX than radiation alone (Fig. 2D). Cell cycle analysis showed that radiation caused G2/M phase arrest, which was exacerbated by the addition of 20 μM EIPA (Fig. 2E and F). These findings suggest that inhibiting NHE1 may make cancer cells more vulnerable to radiation by delaying the recognition of DNA damage and cell cycle re-entry.

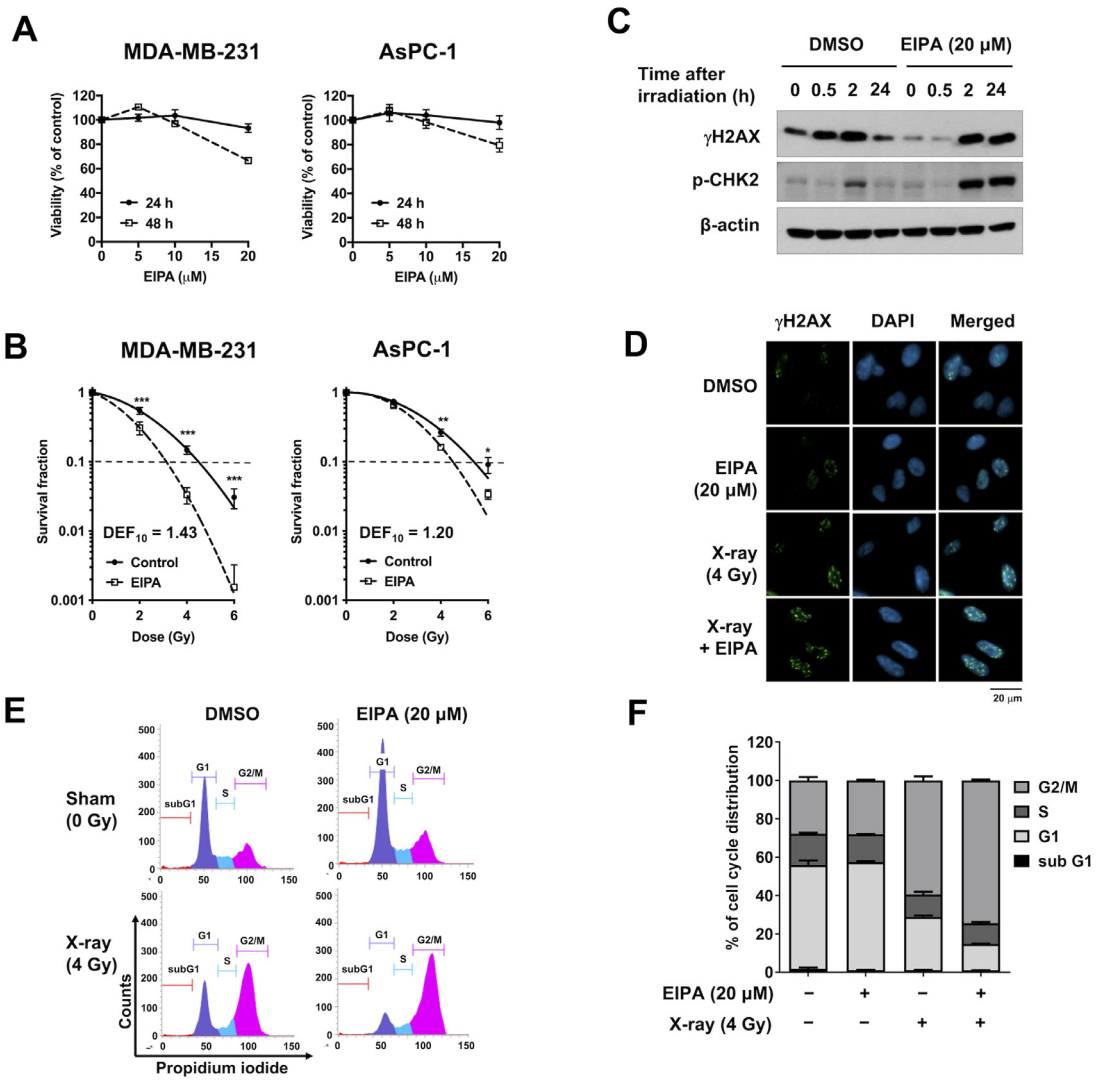

Fig. 2. NHE1 inhibition increases radiation sensitivity in MDA-MB-231 and AsPC-1 cells. (A) Effect of EIPA on MDA-MB-231 and AsPC-1 cell viability. The CCK-8 assay was performed to assess cell viability. (B) Clonogenic survival assay of MDA-MB-231 and AsPC-1 cells treated with or without 5 μM EIPA and then exposed to 2, 4, and 6 Gy X-rays. The data represent the mean ± SD (n = 3). ** $p < 0.01$, *** $p < 0.001$. (C) Western blot analysis showed that EIPA attenuated DNA damage response. β-actin was used as a loading control. (D) Representative immunofluorescence images of γ-H2AX foci in MDA-MB-231 nuclei. Cells were treated with 20 μM EIPA for 3 h before being exposed to 4 Gy of X-rays. After 24 h, the cells were fixed and stained. (E) EIPA augmented radiation-induced G2/M arrest. Representative histograms were presented. MDA-MB-231 cells were incubated with 20 μM EIPA for 3 h before being exposed to 4 Gy irradiation. Cell cycle progression was examined 24 h after irradiation. (F) Cell cycle phase quantification. The data represent the mean ± SD (n = 3).

Pharmacological inhibition of NHE1 enhances radiation-induced apoptosis in MDA-MB-231 cells

We next determined the effect of the NHE1 inhibitor on radiation-induced apoptosis, one of the radiation-induced cell death modes. Flow cytometry with Annexin V/PI co-staining revealed that high concentrations of EIPA (above 50 μM) increased apoptotic cell death (Fig. 3A and B). When compared to X-ray alone, the combination of 20 μM EIPA and 4 Gy of X-ray significantly increased apoptosis ($p < 0.01$) compared with X-ray alone (Fig. 3C). With EIPA or X-ray, the caspase Glo 3/7 assay showed a dose-dependent increase in caspase 3/7 activity (Fig. 3D and E). When combined with 4 Gy or 6 Gy of X-ray, pre-treatment with 20 μM EIPA increased caspase 3/7 activity even more than sham treatment (Fig. 3F). Western blot analysis confirmed an increase in apoptosis in the cells co-treated with EIPA and X-ray, as determined by cleaved PARP expression (Fig. 3G). The combined treatment reduced the expression of the anti-apoptotic protein MCL-1 while increasing the expression of pro-apoptotic BAK (Fig. 3G). Furthermore, radiation increased the phosphorylation of NF-κB p65, which is associated with pro-survival activity, which was reversed by EIPA treatment (Fig. 3G and H). These data suggest that inhibiting NHE1 promotes radiation-induced apoptosis by suppressing pro-survival signaling.

Knockdown of NHE1 increases radiation sensitivity in MDA-MB-231 cells

It was recently reported that long-term treatment with EIPA has an anticancer effect in 3D culture, independent of NHE1 [35]. To verify whether the radiosensitizing of EIPA was NHE1-dependent, we silenced NHE1 expression in MDA-MB-231 cells using RNA interference. As with EIPA treatment, NHE1 depletion with siRNA decreased pH_i (Fig. 4A). NHE1 knockdown significantly reduced clonogenic cell survival in response to radiation (Fig. 4B). Immunoblotting showed that the expression of γ-H2AX was delayed in NHE1-knockdown cells, compared to cells transfected with control siRNA (Fig. 4C). Radiation-induced apoptosis was increased significantly more in NHE1-knockdown cells than in control siRNA cells ($p < 0.001$), as determined by flow cytometry analy-

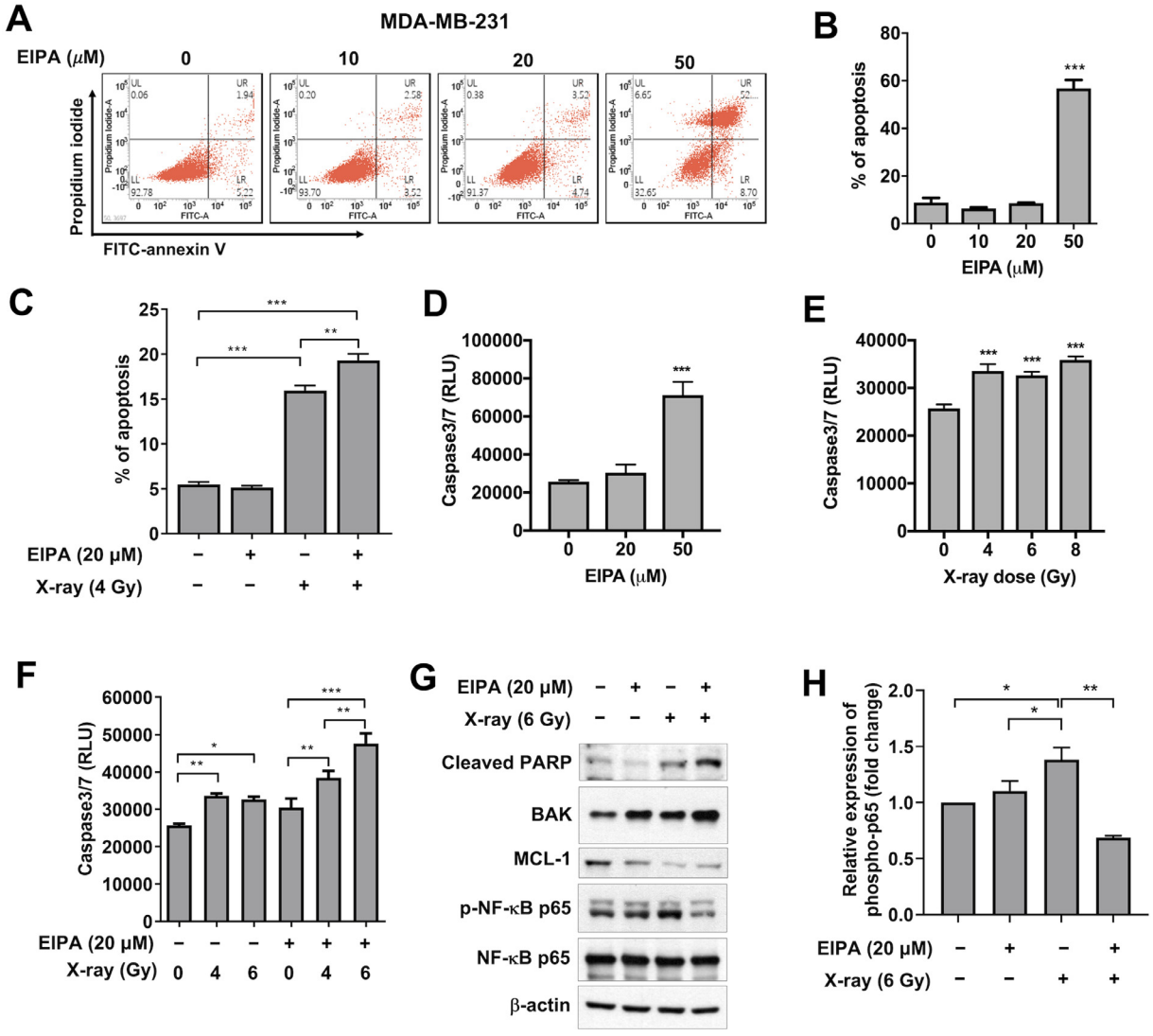

Fig. 3. NHE1 inhibition enhances radiation-induced apoptosis in MDA-MB-231 cells. (A) Flow cytometry diagrams of apoptotic cells co-stained with PI and FITC-annexin. (B) Quantification results showed that 50 μM EIPA induced apoptotic cell death. (C) EIPA increased radiation-induced apoptosis. (D) The Caspase-Glo 3/7 assay demonstrated that 50 μM EIPA induced caspase-dependent apoptosis. (E) Radiation increased the caspase 3/7 activity. (F) EIPA increased radiation-induced caspase 3/7 activity. (G) Western blot analysis showed that EIPA increased radiation-induced apoptotic cell death, as measured by increased PARP cleavage. β-actin was used as a loading control. (H) Quantification of phosphorylated NF-κB p65 using ImageJ. The band intensity was normalized to β-actin. All data represent mean ± SD (n ≥ 3). * $p < 0.05$, ** $p < 0.01$, *** $p < 0.001$.

sis with Annexin V/PI co-staining (Fig. 4 D and E). Treatment with NHE1 siRNA abolished the radiation-induced NHE1 expression and increased the expression of γ-H2AX and cleaved PARP (Fig. 4F). These data suggest that EIPA radiosensitizes cancer cells dependently on NHE1.

Inhibition of NHE1 augments radiation-induced tumor growth delay in an MDA-MB-231 xenograft mouse model

To test whether inhibition of NHE1 exerts its radiosensitizing effect in vivo, we inoculated MDA-MB-231 cells in the right hind legs of BALB/c nude mice and treated the xenograft tumors with radiation and EIPA (Fig. 5A). Either EIPA or 6 Gy of X-ray irradiation attenuated the growth of MDA-MB-231 tumors, although the difference was not statistically significant (Fig. 5B). The combination of radiation and EIPA significantly inhibited tumor growth compared to sham treatment or radiation alone (Fig. 5B). Bodyweight did not change during the treatments, and no visible toxic effect was seen (Fig. 5C). Tumors were harvested 54 days after irradiation for further analysis. The TUNEL assay of tumor tissues revealed that either EIPA or IR alone slightly increased the apoptotic cell population, which was markedly increased by the combination treatment (Fig. 5D and E). Next, we tested how radiation or EIPA affects NHE1 and p-NF-κB p65 levels in the tumor tissues using immunohistochemical (IHC) staining. A single dose of radiation significantly increased the abundance of NHE1 and phospho-NF-κB p65 in the tumor tissues, which was suppressed by EIPA co-treatment (Fig. 5F, G, and H). Our data indicate that NHE1 inhibition further attenuated the growth of the irradiated tumors, which may be related to a decreased pro-survival signaling, including NF-κB with increased apoptotic cell death.

Radioresistant MDA-MB-231 cells have increased NHE1 and phosphorylation of NF-κB

To determine whether NHE1 contributes to acquired radioresistance, we created a radioresistant MDA-MB-231 cell line and investigated NHE1-mediated signaling. A pool of survived cells was collected and named MDA-MB-231RR after a total of 40 Gy was delivered to the cells (five fractions of 2 Gy and four fractions of 5 Gy) (Fig. 6A).

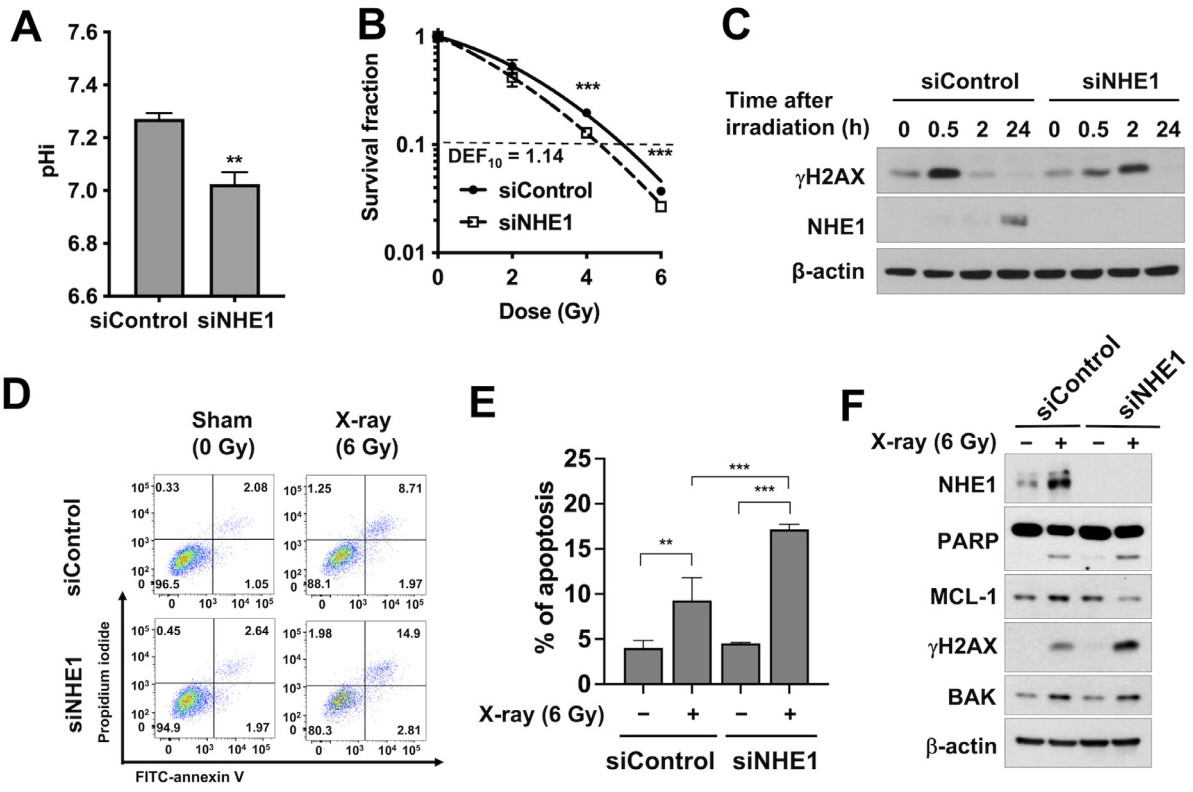

Fig. 4. Knockdown of NHE1 increased radiation sensitivity in MDA-MB-231 cells. (A) NHE1 knockdown decreased pH_i. (B) NHE1 knockdown reduced clonogenic survival in response to X-ray irradiation. (C) Western blot analysis showed delayed expression of γ-H2AX in NHE1-knockdown cells. β-actin was used as a loading control. (D) Representative flow cytometry diagram showing induction of apoptosis in irradiated NHE1-knockdown cells. (E) Quantification data showing enhancement of radiation-induced apoptosis by NHE1 knockdown. All data represent mean ± SD (n ≥ 3). ** $p < 0.01$, *** $p < 0.001$. (F) Western blot analysis showed that NHE1 siRNA depleted NHE1 expression, increased radiation-induced expression of cleaved PARP and γ-H2AX, and decreased MCL-1 expression. The samples were prepared 72 h post-irradiation.

The clonogenic assay confirmed that MDA-MB-231RR cells were significantly more radioresistant than parental cells (Fig. 6B). MDA-MB-231RR cells had increased pH_i compared to the MDA-MB-231 cells (Fig. 6C). As with increased pH_i, radioresistant cells expressed higher levels of NHE1 and phospho-NF-κB p65 but not MCT1 (Fig. 6D). MDA-MB-231RR cells were more sensitive to EIPA than their parental cells in a colony formation assay (Fig. 6E). EIPA treatment reduced clonogenic survival of irradiated MDA-MB-231RR cells, indicating that EIPA re-sensitized MDA-MB-231RR cells to radiation (Fig. 6F). EIPA treatment reduced NHE1 and phospho-NF-κB p65 levels in MDA-MB-231RR cells (Fig. 6G). EIPA treatment also inhibited the activity of NF-κB-dependent luciferase in a dose-dependent manner (Fig. 6H). NHE1 knockdown also decreased the expression of both NHE1 and phospho-NF-κB p65 in MDA-MB-231RR cells (Fig. 6I).

Inhibition of NHE1 induces transcriptomic changes to overcome radioresistance in MDA-MB-231

We used RNA sequencing profiles to determine the transcriptomic changes of MDA-MB-231 (WT), MDA-MB-231RR (RR), and EIPA-treated MDA-MB-231RR cells (EIPA + RR) (Fig. 7A). We identified 490 significant Up/Down DEGs for radioresistant cells (RR versus WT). These RR genes had a significant (p = 1.5e-05) overlap with the genes from RadiationGeneSigDB [36], which contains curated radiation response-related gene signatures (Fig. S2A). The up-regulated genes are enriched in pathways related to cellular senescence, immune, and extracellular matrix (ECM), all of which have been shown to contribute to radioresistance [37,38]. Notably, EIPA significantly reduced the expression of senescence and ECM pathway genes, implying that the radioresistant status was alleviated at the transcriptome level (Fig. 7B).

To confirm transcription factors (TFs) that may potentially be involved in radioresistance and EIPA-induced sensitization, we performed enrichment analysis against a known 790 TF downstream geneset collected in Harmonizome [29], similar to conventional pathway analysis (Fig. 7C). NF-κB and its associated regulators, such as LYL1, HTT, TRAF4, and IRF7 [39,40] were among the top 20 TFs. TGFβ and epithelial-mesenchymal transition (EMT) regulators were also highly ranked, and these TFs are known to play a key role in radioresistance [41]. EIPA treatment significantly downregulated the expression of the majority of these TF downstream genes in the RR cells. Some of these TFs may be involved in the establishment of radioresistance and EIPA-induced sensitization in the RR cells.

Using STRING gene network [30], we investigated the interactions of signature genes from three key processes (NF-κB, ECM, and senescence) and found that the signature genes were tightly linked (Fig. 7D). The connectivity of signature genes (network density = 1.5e-02) was 20 times denser than that of the random genes in STRING network (mean network density = 6.9e-03, $p < 0.001$ estimated by 1000 times of random sampled networks of the same size). EIPA treatment frequently down-regulated, or "flipped," up-regulated genes in MDA-MB-231RR cells. For example, IL6 and CXCL1 were significantly higher in RR cells, which were reversed by EIPA (Fig. 7D). We also analyzed EIPA dose-dependent changes in these 'Flip genes'. Like the pathway analysis, 'Flip genes' were significantly enriched with the three key processes and other signaling pathways. Furthermore, most of these pathways were significantly enriched with genes from RadiationGeneSigDB (Fig. S2B). Overall, inhibiting NHE1 appears to facilitate transcriptomic changes that reverse the expression pattern of radioresistance-associated genes and pathways.

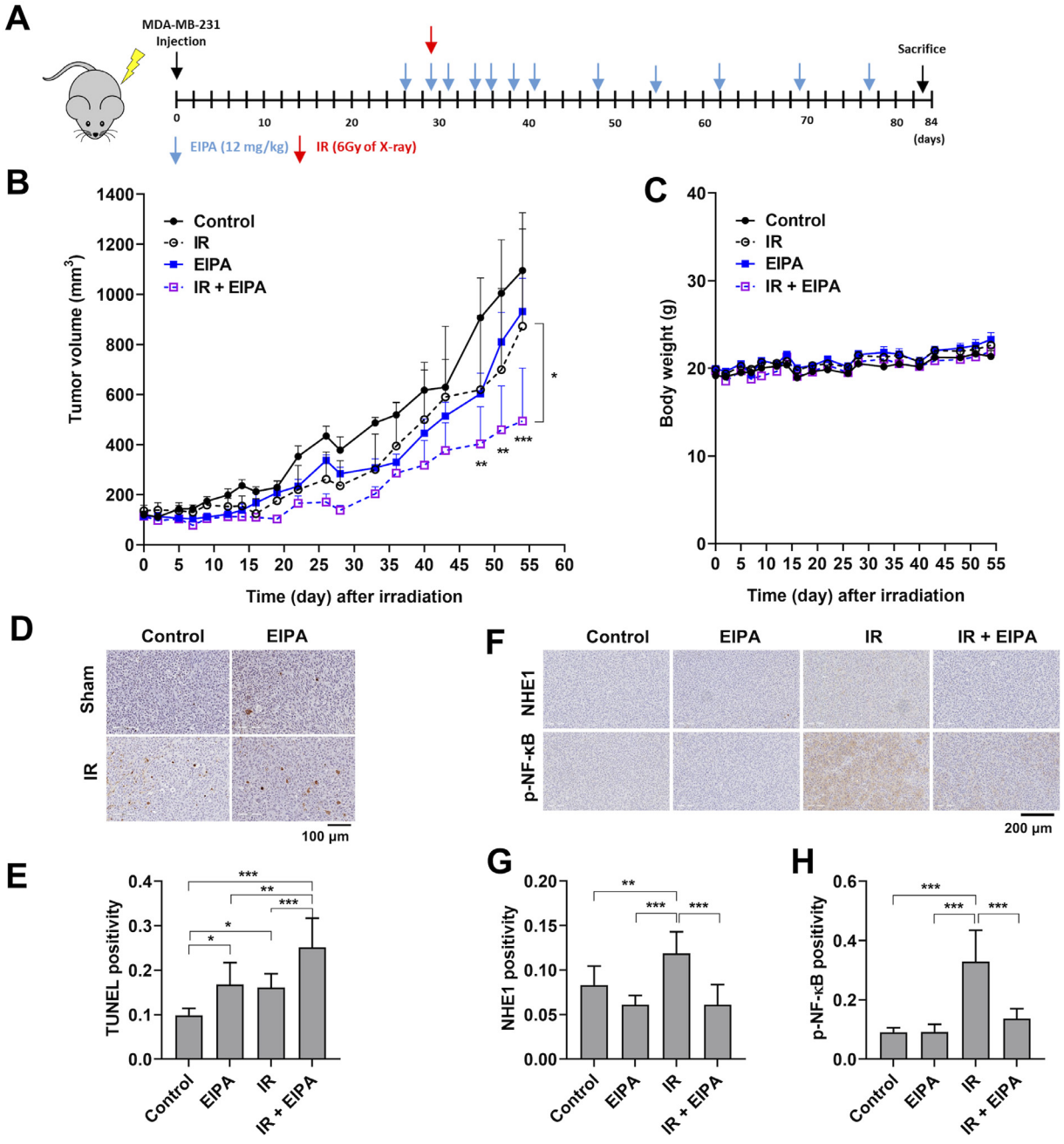

Fig. 5. NHE1 inhibition increases radiation-induced tumor growth delay *in vivo*. (A) Treatment scheme for ionizing radiation (IR) and EIPA in an MDA-MB-231 tumor xenograft model. (B) MDA-MB-231 xenograft tumor growth curves in mice treated with EIPA and IR. The data represent the mean ± SD (n = 5). (C) Changes in mouse body weight during treatments. (D) Representative TUNEL staining images of the MDA-MB-231 tumor tissues. Tumors were harvested 54 days after irradiation. (E) TUNEL positivity quantification. (F) Representative immunohistochemistry images of NHE1 and phospho-NF-κB p65 in MDA-MB-231 tumor tissues. (G) NHE1 expression quantification. (H) phospho-NF-κB p65 expression quantification. The data represent the mean ± SD (n = 9). * $p < 0.05$; ** $p < 0.01$; *** $p < 0.001$.

Radioresistance-associated pathways show a positive correlation with NHE1 expression in TNBC patients

In order to validate the clinical relevance of NHE1 for radioresistance, we analyzed the transcriptome and the survival of TNBC patients extracted from the breast cancer dataset of TCGA (Fig. S3A). Of the 1222 BRCA samples, 239 patients were annotated as TNBC according to FPKM of ERBB2, ESR1, and PGR (Materials and methods). These 239 TNBC patients were classified as NES-high and –low groups depending on the expression level of the three key processes listed in Fig. 7B. The NES-high group showed a significantly higher expression of NHE1 (p = 3.2e-04) (Fig. S3B). Furthermore, only the patients who received radiotherapy (n = 123) showed a significant difference between NES-high and –low groups in survival (Fig. S3C), where the NES-low group showed better overall survival, although only mild (p = 3.8e-02). The survival difference was not observed in the patients without radiotherapy (n = 81). Our observation suggests that high NHE1 expression is likely to be associated with poor survival among RT-treated patients possibly through up-regulation of the radioresistance-associated processes.

Discussion

Radiation therapy is one of the most effective standard cancer treatments. Recent radiation technique advancements, such as image-guided

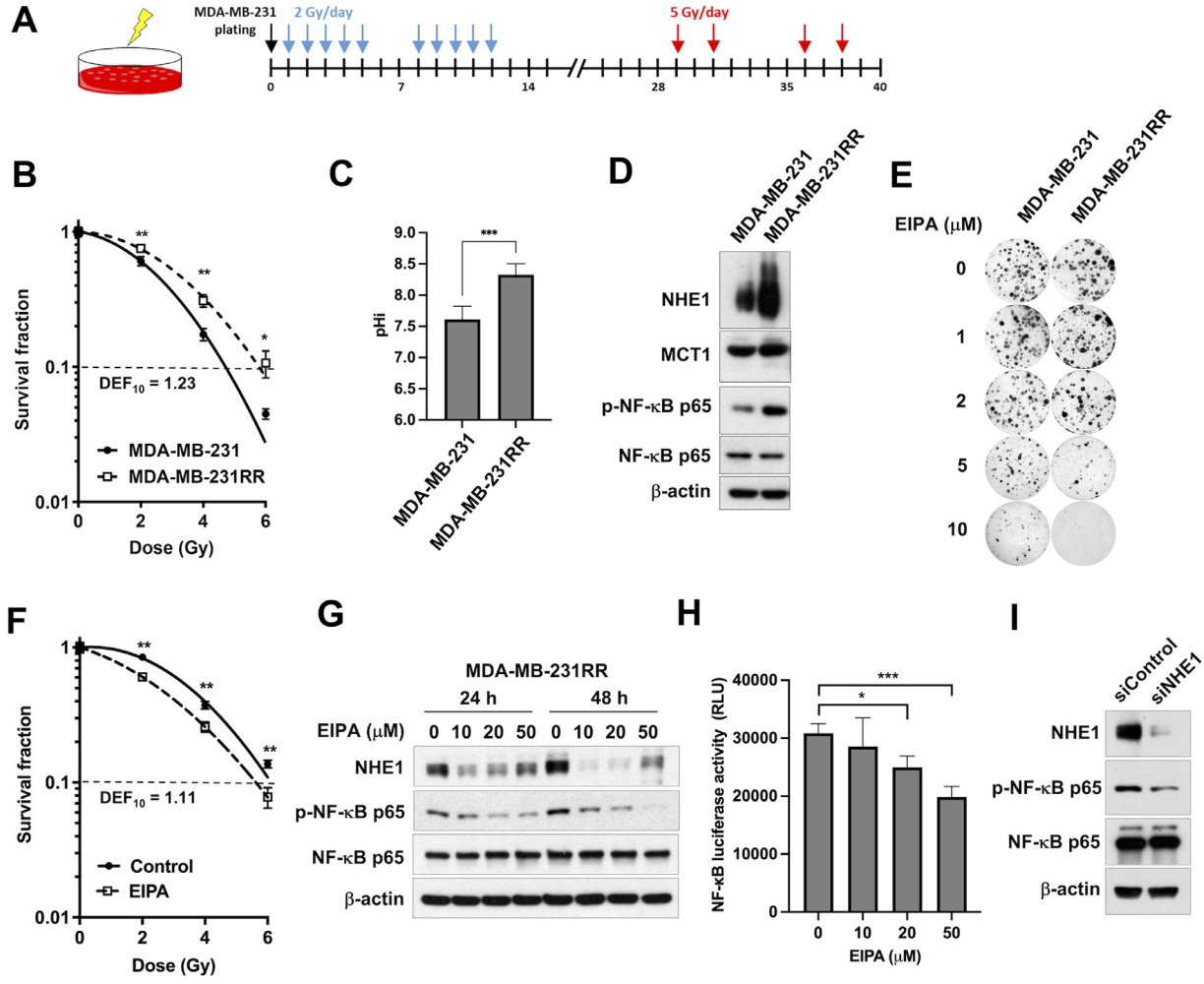

Fig. 6. NHE1 expression and NF-κB activation are increased in radioresistance MDA-MB-231 cells. (A) Scheme for establishing radioresistant MDA-MB-231 cells (MDA-MB-231RR). Cells that survived 40 Gy of X-rays were pooled and subjected to a clonogenic assay. (B) A clonogenic assay showed that MDA-MB-231RR cells were radioresistant compared to their parental cells. The data represent the mean ± S.D (n = 3). * $p < 0.05$; ** $p < 0.01$. (C) MDA-MB-231RR cells had increased pH_i compared to parental cells. The data represent the mean ± S.D (n = 8). *** $p < 0.001$. (D) Western blot analysis showed that NHE1 but not MCT1 was induced in MDA-MB-231RR cells. The phosphorylation of NF-κB p65 was also increased. β-actin was used as a loading control. (E) MDA-MB-231RR cells were more susceptible to EIPA than parental cells. (F) Treatment with EIPA re-sensitized MDA-MB-231RR cells to radiation. 5 μM EIPA was pre-treated. (G) EIPA treatment reduced the expression of phospho-NF-κB p65 in a dose-dependent manner. (H) EIPA inhibited NF-κB-dependent luciferase activity. The data represent the mean ± S.D (n = 4). * $p < 0.05$; *** $p < 0.001$. (I) NHE1 knockdown also decreased the expression of phospho-NF-κB p65.

radiotherapy and particle beam therapy, have resulted in better tumor control while minimizing normal tissue damage. Nonetheless, tumor cells frequently develop radiation resistance during the treatment, which can lead to repopulation and cancer relapse. Understanding how tumor cells acquire radiation resistance is therefore critical for improving treatment outcomes. Although dysregulated pH_i is linked to cancer, its role in radioresistance is largely unknown. We propose in this paper that targeting NHE1, a key regulator of pH_i, is a previously unrecognized but effective strategy for overcoming radioresistance.

Preclinical investigation of NHE1 inhibitors has been conducted as anti-cancer drugs in pancreatic cancer [16], and fibrosarcoma [17] models. Our findings consistently demonstrated that EIPA, an NHE1 inhibitor, decreased the viability of two cancer cell lines. EIPA significantly enhanced radiation-induced cell eradication in MDA-MB-231 and AsPC-1 cells. Radiation also inhibited the growth of 3D-cultured MDA-MB-231 and AsPC-1 spheroids, which was further inhibited by the addition of EIPA. EIPA decreased pH_i in a concentration-dependent manner. A low dose of IR such as 2 Gy raised pH_i. NHE1 activity is regulated by the direct phosphorylation of AKT and ERK on its C-terminal tail [18,42]. We speculated that low-dose irradiation may activate AKT or ERK, resulting in an increase in pH_i which is likely to provide a survival signal. On the contrary, high doses above 6 Gy decreased pH_i, despite increased NHE1 expression. This may be due to mitochondrial dysfunction and reactive oxygen species (ROS) production, which is known to be associated with apoptosis-mediated intracellular acidification [5]. The addition of EIPA to high-dose X-ray resulted in an even lower pH_i, potentially inhibiting growth inhibition and cell death. The specificity of EIPA for NHE1 inhibition was supported by NHE1 knockdown experiments. These findings suggest that radiation may affect NHE1-regulated pH_i homeostasis. Further investigation will help to understand how radiation regulates NHE1 activity or expression. Direct measurement of NHE1 activity using NH_4^+ prepulse could inform about such effects.

Ionizing radiation causes DNA damage and cell cycle arrest, and the accumulation of irreparable DNA damage results in cell death. Delayed expression of γ-H2AX and phosphorylated CHK2 indicated that EIPA attenuated radiation-induced DNA damage repair. Immunostaining of γ-H2AX revealed more foci in EIPA-treated irradiated cells than in DMSO-treated irradiated cells. Cell cycle analysis further confirmed that EIPA increased the radiation-induced G2/M arrest. Previous research has shown that an NHE1-dependent increase in pH_i is required

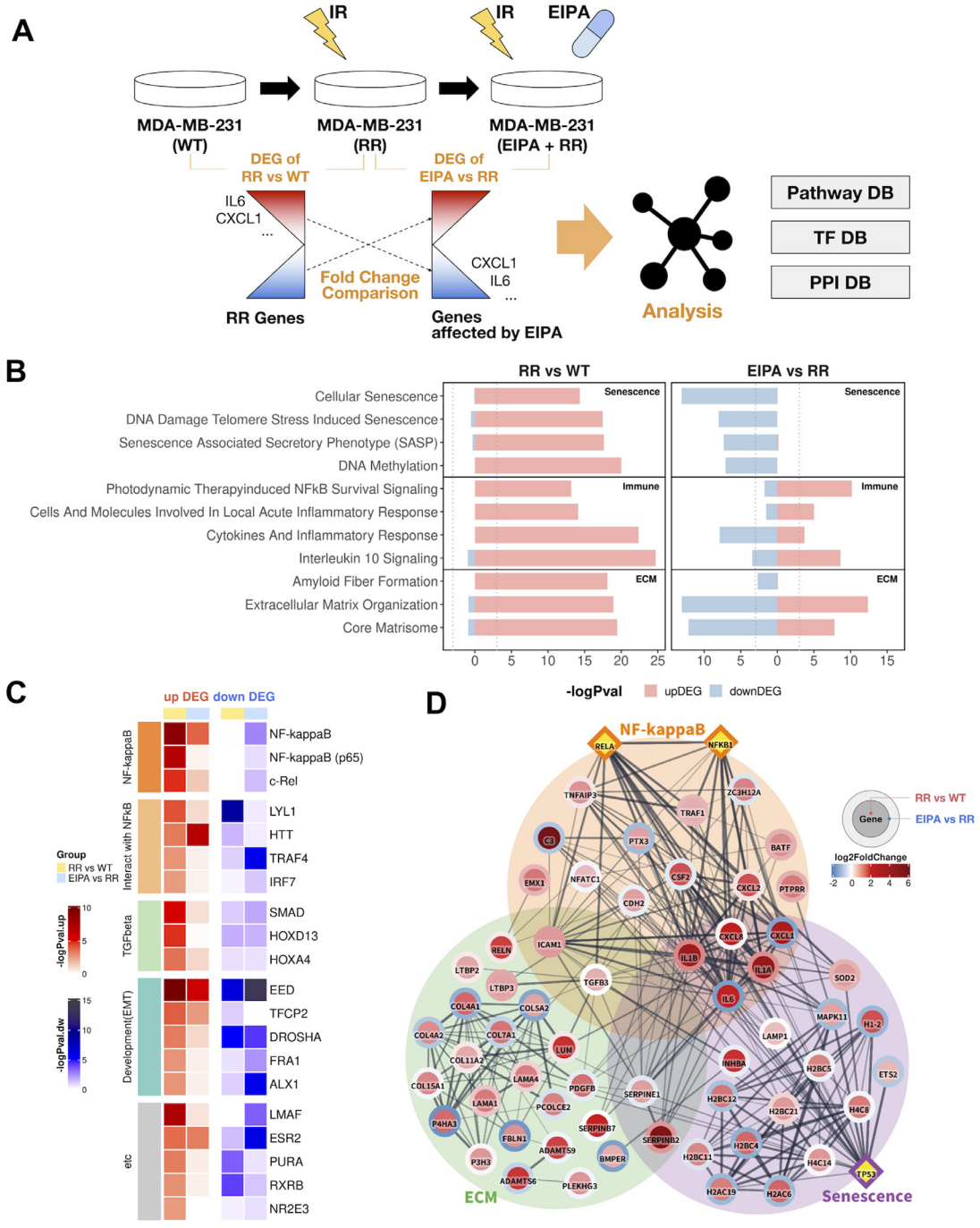

Fig. 7. Pharmacological inversion of radioresistance-associated expression patterns in MDA-MB-231 cells by NHE1 inhibition. (A) An overview of transcriptome analyses of radioresistant MDA-MB-231 cells treated with EIPA. Gene expression of MDA-MB-231RR and EIPA-treated RR cells was profiled, and signature genes for pathways, transcription factors (TFs), and protein-protein-interaction (PPI) networks were identified. (B) Pathways enriched in RR cells (RR versus WT) and EIPA-treated RR cells (EIPA versus RR) related to several key processes, including senescence, immune, and ECM. Pathways that are up- or down-regulated are colored in red or blue, respectively. P-values are calculated by the hypergeometric test, and the dotted lines indicate a significance cut-off ($p < 0.05$, hypergeometric test). (C) TF analysis for signature genes that are up- or down-regulated. The top 20 most significant TFs are organized into known functional classes. The significance of enrichment was calculated using a hypergeometric test, and 790 TF downstream genesets were obtained from Harmonizome. (D) Signature gene network in the three key processes (NF-κB, ECM, and senescence). The networks were taken from STRING with a confidence score > 0.4. Signature genes are denoted by circles, and additional TFs are denoted by diamonds (RELA, NFKB1, and TP53). The inner color of a node represents the expression change in RR vs WT group, and the outer color represents the expression change in the EIPA versus RR group.

for G2/M entry [4], and NHE1 inhibition reduced the expression of components required for G2/M transition, such as cyclin B1, which may explain the prolonged G2/M arrest after irradiation and EIPA. In human leukemia HL-60 cells, amiloride, a prototype of EIPA, reduced the radiation-induced G2 block, resulting in delaying apoptosis [43], which suggests the effect of amiloride derivatives on the cell cycle is cell context-dependent.

NHE1 inhibition increased radiation-induced apoptosis. At 50 μM, EIPA alone significantly increased caspase 3/7 activity but was no longer NHE1-specific as no apoptotic induction was observed in NHE1-

knockdown cells. When combined with radiation, EIPA pre-treatment increased caspase 3/7 activity even at 20 μM. EIPA plus X-ray increased apoptotic markers cleaved PARP and BAK while decreasing the anti-apoptotic protein MCL-1. The combination of EIPA and X-ray reduced the phosphorylated form of NF-κB p65 but not the total protein. EIPA or radiation alone inhibited the growth of MDA-MB-231 tumors in a xenograft tumor mouse model. Co-administration with EIPA inhibited the growth of irradiated tumors even more. The TUNEL assay revealed that EIPA increased apoptosis in tumor tissues exposed to radiation, which was consistent with our in vitro findings. Furthermore, radiation increased the expression of NHE1 and phosphorylated NF-κB p65 in tumor tissues, which was suppressed by EIPA co-administration. These findings suggest that blocking NHE1 may have a radiosensitizing effect by increasing apoptosis, which may be involved in the suppression of NF-κB signaling.

NF-κB is one of the transcription factors linked to radiation resistance, including signals transduces and activator of transcription 3 (STAT3), nuclear factor (erythroid-derived-2)-like 2 (NRF2), and hypoxia-inducible factor-1 (HIF-1). Numerous genes involved in diverse cellular functions, such as cell proliferation, survival, and inflammation, are regulated by NF-κB. In terms of radioresistance, ionizing radiation activates NF-κB signaling via DNA damage-mediated ATM activation, cytokine-mediated tumor necrosis factor receptor (TNF) signaling, or ROS-mediated AKT activation [44]. Activated NF-κB increases the expression of antioxidant genes like mitochondrial manganese superoxide dismutase (MnSOD), anti-apoptotic genes like BCL-2 and BCL-xL, and EMT-related genes like COX-2 and MMP1. To better understand the underlying mechanism of NHE1-mediated radioresistance, we created a radioresistant MDA-MB-231 cell line and performed a whole transcriptomic analysis. Radioresistant cells had a higher level of NHE1, pH_i, and phosphorylated NF-κB p65 than control cells. The radioresistant cells were more sensitive to EIPA than their parental cells, which could be attributed to a decrease in NHE1 and phosphorylated NF-κB p65 abundance. Gene expression profiling confirmed that the NF-κB pathway, along with senescence and ECM, was one of the core pathways activated in the radioresistant group. Furthermore, comparative transcriptome analysis on EIPA-treated cells demonstrated that blocking NHE1 reversed NF-κB activation in radioresistant cells, implying a role for NHE1 and NF-κB in adaptive radioresistance.

Little is known about how NHE1 or pH_i modulates NF-κB signaling in the presence of radiation. In normal tissues such as human umbilical endothelial vein cells and gut epithelial cells, blocking NHE1 inhibited the NF-κB pathway, resulting in suppressing the inflammatory response [45]. NHE1 inhibition re-sensitizes chemoresistant MCF7 cancer cells to doxorubicin via apoptosis activation and NF-κB p65 downregulation [46]. This is consistent with our findings that NHE1 inhibition abrogated increased NHE1 and NF-κB activation in the irradiated and radioresistant MDA-MB-231 cells. Aside from the NF-κB pathway, our bioinformatics analyses revealed that TGFβ, EMT, and ECM genes were upregulated in radioresistance cells, which were related to metastatic potential. TGFβ induces a SMAD4-dependent increase in NHE1 and pH_i during EMT in Panc-1 pancreatic cancer cells [47]. EMT-driven invasion necessitates NHE1 transcriptional upregulation via the EMT-TF Zeb1 [48]. Hypoxia-mediated EMT and migration/invasion of MDA-MB-231 cells were inhibited by NHE1 inhibition [49,50]. Thus, inhibiting NHE1 could reduce metastatic potential by preventing radiation-induced EMT.

Our study has several limitations. Although NHE1 is a primary pH_i regulator, it remains unclear whether the radiosensitizing effect of targeting NHE1 activity is directly dependent on pHi. Inhibition of other pH modifiers, such as MCTs, should be tested to determine whether the results depend on either NHE1 or pH_i. Recent optogenetics tools will be useful for testing the direct effect of pHi changes on radiation sensitivity [51]. The absolute pH_i value of MDA-MB-231 cells was relatively lower than that of most cancer cells, and inter-experimental variation was also observed. Nonetheless, the pH probes used were adequate for comparing relative pH_i changes, and future research will look into other pH-specific probes for this purpose. Another limitation is that intraperitoneal administration of EIPA in the MDA-MB-231 xenograft mouse model makes it difficult to determine whether EIPA affects tumor cells in the tumor microenvironment directly or indirectly. A xenograft model using NHE1 knockout cells could be a more effective way to determine the direct role of NHE1 in radiosensitization. Finally, transcriptomic analysis of the WT + EIPA group is important to confirm that the TF downstream genes downregulated by EIPA are not dependent on the distinct characteristics of RR cells.

Given that adaptive radioresistance may be a major cause of tumor recurrence, understanding how tumor cells acquire radioresistance is critical for overcoming radiotherapy local failure. Our findings show that NHE1 is adaptively upregulated during radiation treatment and highly enriched in the cells with acquired radioresistance. In addition to NF-κB, NHE1 inhibition reversed radiation-induced senescence, suggesting that NHE1 inhibition exerts a senolytic effect to eliminate senescent cells. These radioresistance-associated signaling networks were found to be associated with high NHE1 expression in TNBC patient samples from the TCGA database, which seemed to be RT-specific. Further investigation in multiple patient cohorts will be required to validate the clinical significance of NHE1 expression in RT response. In conclusion, our integrated approach using in vitro, in vivo, and in silico methods suggests that targeting NHE1 could be a promising therapeutic strategy for improving RT efficacy.

Data availability statement

All data generated and analyzed during this research are present in the paper and/or in the supplementary materials.

Declaration of Competing Interest

All authors have declared no conflict of interest.

CRediT authorship contribution statement

Arang Son: Validation, Formal analysis, Investigation, Data curation. **Seoyeong Kang:** Validation, Investigation, Visualization. **Suha Choi:** Investigation, Formal analysis. **Sung-Won Shin:** Investigation, Data curation. **Yeeun Kim:** Investigation, Validation. **Wankyu Kim:** Resources, Writing – review & editing, Supervision, Funding acquisition. **Changhoon Choi:** Conceptualization, Writing – original draft, Writing – review & editing, Project administration, Funding acquisition.

Acknowledgments

This work was supported by grants from the National Research Foundation of Korea (NRF), funded by the Korean government (NRF-2021R1F1A1062064, NRF-2021M3H9A2098572 and NRF-2018R1D1A1B07042738).

Supplementary materials

Supplementary material associated with this article can be found, in the online version, at doi:10.1016/j.neo.2022.100862.

References

[1] B.A. Webb, M. Chimenti, M.P. Jacobson, D.L. Barber, Dysregulated pH: a perfect storm for cancer progression, Nat. Rev. Cancer 11 (2011) 671–677.
[2] K.A. White, B.K. Grillo-Hill, D.L. Barber, Cancer cell behaviors mediated by dysregulated pH dynamics at a glance, J. Cell Sci. 130 (2017) 663–669.
[3] C. Corbet, O. Feron, Tumour acidosis: from the passenger to the driver's seat, Nat. Rev. Cancer 17 (2017) 577–593.
[4] L.K. Putney, D.L. Barber, Na-H exchange-dependent increase in intracellular pH times G2/M entry and transition, J. Biol. Chem. 278 (2003) 44645–44649.
[5] D. Lagadic-Gossmann, L. Huc, V. Lecureur, Alterations of intracellular pH homeostasis in apoptosis: origins and roles, Cell Death Differ. 11 (2004) 953–961.

[6] S. Matsuyama, J. Llopis, Q.L. Deveraux, R.Y. Tsien, J.C. Reed, Changes in intramitochondrial and cytosolic pH: early events that modulate caspase activation during apoptosis, Nat. Cell Biol. 2 (2000) 318–325.

[7] B.A. Webb, F. Forouhar, F.E. Szu, J. Seetharaman, L. Tong, D.L. Barber, Structures of human phosphofructokinase-1 and atomic basis of cancer-associated mutations, Nature 523 (2015) 111–114.

[8] C.H. Choi, B.A. Webb, M.S. Chimenti, M.P. Jacobson, D.L. Barber, pH sensing by FAK-His58 regulates focal adhesion remodeling, J. Cell Biol. 202 (2013) 849–859.

[9] C. Stock, B. Gassner, C.R. Hauck, H. Arnold, S. Mally, J.A. Eble, P. Dieterich, A. Schwab, Migration of human melanoma cells depends on extracellular pH and Na+/H+ exchange, J. Physiol. 567 (2005) 225–238.

[10] B.T. Beaty, Y. Wang, J.J. Bravo-Cordero, V.P. Sharma, V. Miskolci, L. Hodgson, J. Condeelis, Talin regulates moesin-NHE-1 recruitment to invadopodia and promotes mammary tumor metastasis, J. Cell Biol. 205 (2014) 737–751.

[11] R. Xie, H. Wang, H. Jin, G. Wen, B. Tuo, J. Xu, NHE1 is upregulated in gastric cancer and regulates gastric cancer cell proliferation, migration and invasion, Oncol. Rep. 37 (2017) 1451–1460.

[12] H. Wang, X. Long, D. Wang, M. Lou, D. Zou, R. Chen, W. Nian, Q. Zhou, Increased expression of Na(+)/H(+) exchanger isoform 1 predicts tumor aggressiveness and unfavorable prognosis in epithelial ovarian cancer, Oncol. Lett. 16 (2018) 6713–6720.

[13] X. Guan, L. Luo, G. Begum, G. Kohanbash, Q. Song, A. Rao, N. Amankulor, B. Sun, D. Sun, W. Jia, Elevated Na/H exchanger 1 (SLC9A1) emerges as a marker for tumorigenesis and prognosis in gliomas, J. Exp. Clin. Cancer Res. 37 (2018) 255.

[14] D. Rotin, D. Steele-Norwood, S. Grinstein, I. Tannock, Requirement of the Na+/H+ exchanger for tumor growth, Cancer Res. 49 (1989) 205–211.

[15] S.R. Amith, J.M. Wilkinson, S. Baksh, L. Fliegel, The Na(+)/H(+) exchanger (NHE1) as a novel co-adjuvant target in paclitaxel therapy of triple-negative breast cancer cells, Oncotarget 6 (2015) 1262–1275.

[16] C. Commisso, S.M. Davidson, R.G. Soydaner-Azeloglu, S.J. Parker, J.J. Kamphorst, S. Hackett, E. Grabocka, M. Nofal, J.A. Drebin, C.B. Thompson, J.D. Rabinowitz, C.M. Metallo, M.G. Vander Heiden, D. Bar-Sagi, Macropinocytosis of protein is an amino acid supply route in Ras-transformed cells, Nature 497 (2013) 633–637.

[17] M. Yamagata, I.F. Tannock, The chronic administration of drugs that inhibit the regulation of intracellular pH: in vitro and anti-tumour effects, Br. J. Cancer 73 (1996) 1328–1334.

[18] G. Lauritzen, M.B. Jensen, E. Boedtkjer, R. Dybboe, C. Aalkjaer, J. Nylandsted, S.F. Pedersen, NBCn1 and NHE1 expression and activity in DeltaNErbB2 receptor-expressing MCF-7 breast cancer cells: contributions to pHi regulation and chemotherapy resistance, Exp. Cell. Res. 316 (2010) 2538–2553.

[19] R.A. Cardone, M.R. Greco, K. Zeeberg, A. Zaccagnino, M. Saccomano, A. Bellizzi, P. Bruns, M. Menga, C. Pilarsky, A. Schwab, F. Alves, H. Kalthoff, V. Casavola, S.J. Reshkin, A novel NHE1-centered signaling cassette drives epidermal growth factor receptor-dependent pancreatic tumor metastasis and is a target for combination therapy, Neoplasia 17 (2015) 155–166.

[20] X. Guan, M.N. Hasan, G. Begum, G. Kohanbash, K.E. Carney, V.M. Pigott, A.I. Persson, M.G. Castro, W. Jia, D. Sun, Blockade of Na/H exchanger stimulates glioma tumor immunogenicity and enhances combinatorial TMZ and anti-PD-1 therapy, Cell Death. Dis. 9 (2018) 1010.

[21] B.M. Bola, A.L. Chadwick, F. Michopoulos, K.G. Blount, B.A. Telfer, K.J. Williams, P.D. Smith, S.E. Critchlow, I.J. Stratford, Inhibition of monocarboxylate transporter-1 (MCT1) by AZD3965 enhances radiosensitivity by reducing lactate transport, Mol. Cancer Ther. 13 (2014) 2805–2816.

[22] C. Corbet, E. Bastien, N. Draoui, B. Doix, L. Mignion, B.F. Jordan, A. Marchand, J.C. Vanherck, P. Chaltin, O. Schakman, H.M. Becker, O. Riant, O. Feron, Interruption of lactate uptake by inhibiting mitochondrial pyruvate transport unravels direct antitumor and radiosensitizing effects, Nat. Commun. 9 (2018) 1208.

[23] W.C. Duivenvoorden, S.N. Hopmans, D. Gallino, T. Farrell, C. Gerdes, D. Glennie, H. Lukka, J.H. Pinthus, Inhibition of carbonic anhydrase IX (CA9) sensitizes renal cell carcinoma to ionizing radiation, Oncol. Rep. 34 (2015) 1968–1976.

[24] J. Doyen, S.K. Parks, S. Marcie, J. Pouyssegur, J. Chiche, Knock-down of hypoxia-induced carbonic anhydrases IX and XII radiosensitizes tumor cells by increasing intracellular acidosis, Front. Oncol. 2 (2012) 199.

[25] A. Dobin, C.A. Davis, F. Schlesinger, J. Drenkow, C. Zaleski, S. Jha, P. Batut, M. Chaisson, T.R. Gingeras, STAR: ultrafast universal RNA-seq aligner, Bioinformatics 29 (2013) 15–21.

[26] B. Li, C.N. Dewey, RSEM: accurate transcript quantification from RNA-Seq data with or without a reference genome, BMC Bioinformat. 12 (2011) 323.

[27] M.I. Love, W. Huber, S. Anders, Moderated estimation of fold change and dispersion for RNA-seq data with DESeq2, Genome Biol. 15 (2014) 550.

[28] A. Liberzon, C. Birger, H. Thorvaldsdóttir, M. Ghandi, J.P. Mesirov, P. Tamayo, The molecular signatures database (MSigDB) hallmark gene set collection, Cell Syst. 1 (2015) 417–425.

[29] A.D. Rouillard, G.W. Gundersen, N.F. Fernandez, Z. Wang, C.D. Monteiro, M.G. McDermott, A. Ma'ayan, The harmonizome: a collection of processed datasets gathered to serve and mine knowledge about genes and proteins, Database (Oxford) 2016 (2016) baw100.

[30] D. Szklarczyk, A.L. Gable, K.C. Nastou, D. Lyon, R. Kirsch, S. Pyysalo, N.T. Doncheva, M. Legeay, T. Fang, P. Bork, L.J. Jensen, C. von Mering, The STRING database in 2021: customizable protein–protein networks, and functional characterization of user-uploaded gene/measurement sets, Nucleic Acids Res. 49 (2021) D605–D612.

[31] P. Shannon, A. Markiel, O. Ozier, N.S. Baliga, J.T. Wang, D. Ramage, N. Amin, B. Schwikowski, T. Ideker, Cytoscape: a software environment for integrated models of biomolecular interaction networks, Genome Res. 13 (2003) 2498–2504.

[32] R.L. Grossman, A.P. Heath, V. Ferretti, H.E. Varmus, D.R. Lowy, W.A. Kibbe, L.M. Staudt, Toward a shared vision for cancer genomic data, N. Engl. J. Med. 375 (2016) 1109–1112.

[33] A. Subramanian, P. Tamayo, V.K. Mootha, S. Mukherjee, B.L. Ebert, M.A. Gillette, A. Paulovich, S.L. Pomeroy, T.R. Golub, E.S. Lander, J.P. Mesirov, Gene set enrichment analysis: a knowledge-based approach for interpreting genome-wide expression profiles, Proceedings of the National Academy of Sciences of the United States of America, 102 (2005) 15545-15550.

[34] A.A. Sergushichev, An algorithm for fast preranked gene set enrichment analysis using cumulative statistic calculation, bioRxiv (2016) 060012.

[35] M.G. Rolver, L.O. Elingaard-Larsen, A.P. Andersen, L. Counillon, S.F. Pedersen, Pyrazine ring-based Na(+)/H(+) exchanger (NHE) inhibitors potently inhibit cancer cell growth in 3D culture, independent of NHE1, Sci. Rep. 10 (2020) 5800.

[36] V.S. Manem, A. Dhawan, RadiationGeneSigDB: a database of oxic and hypoxic radiation response gene signatures and their utility in pre-clinical research, Br. J. Radiol. 92 (2019) 20190198 -20190198.

[37] N. Cordes, V. Meineke, Cell adhesion-mediated radioresistance (CAM-RR). Extracellular matrix-dependent improvement of cell survival in human tumor and normal cells in vitro, Strahlenther. Onkol. 179 (2003) 337–344.

[38] R.R. Gordon, P.S. Nelson, Cellular senescence and cancer chemotherapy resistance, Drug Resistance Updates 15 (2012) 123–131.

[39] M. Iwanaszko, M. Kimmel, NF-κB and IRF pathways: cross-regulation on target genes promoter level, BMC Genomics 16 (2015) 307 -307.

[40] U. Träger, R. Andre, N. Lahiri, A. Magnusson-Lind, A. Weiss, S. Grueninger, C. McKinnon, E. Sirinathsinghji, S. Kahlon, E.L. Pfister, R. Moser, H. Hummerich, M. Antoniou, G.P. Bates, R. Luthi-Carter, M.W. Lowdell, M. Björkqvist, G.R. Ostroff, N. Aronin, S.J. Tabrizi, HTT-lowering reverses Huntington's disease immune dysfunction caused by NFκB pathway dysregulation, Brain 137 (2014) 819–833.

[41] P. Yadav, B.S. Shankar, Radio resistance in breast cancer cells is mediated through TGF-β signalling, hybrid epithelial-mesenchymal phenotype and cancer stem cells, Biomed. Pharmacother. 111 (2019) 119–130.

[42] M.E. Meima, B.A. Webb, H.E. Witkowska, D.L. Barber, The sodium-hydrogen exchanger NHE1 is an Akt substrate necessary for actin filament reorganization by growth factors, J. Biol. Chem. 284 (2009) 26666–26675.

[43] B.L. Sailer, A.M. Barrasso, J.G. Valdez, J.M. Cobo, J.A. D'Anna, H.A. Crissman, Reduction in the radiation-induced late S phase and G2 blocks in HL-60 cell populations by amiloride, an efficient inhibitor of the Na+/H+ transporter, Cancer Res. 58 (1998) 413–420.

[44] A.L. Hein, M.M. Ouellette, Y. Yan, Radiation-induced signaling pathways that promote cancer cell survival (review), Int. J. Oncol. 45 (2014) 1813–1819.

[45] Z.H. Nemeth, E.A. Deitch, Q. Lu, C. Szabo, G. Hasko, NHE blockade inhibits chemokine production and NF-kappaB activation in immunostimulated endothelial cells, Am. J. Physiol. Cell Physiol. 283 (2002) C396–C403.

[46] Q. Chen, Y. Liu, X.L. Zhu, F. Feng, H. Yang, W. Xu, Increased NHE1 expression is targeted by specific inhibitor cariporide to sensitize resistant breast cancer cells to doxorubicin in vitro and in vivo, BMC Cancer 19 (2019) 211.

[47] R.R. Malinda, K. Zeeberg, P.C. Sharku, M.Q. Ludwig, L.B. Pedersen, S.T. Christensen, S.F. Pedersen, TGFbeta signaling increases net acid extrusion, proliferation and invasion in Panc-1 pancreatic cancer cells: SMAD4 dependence and link to merlin/NF2 signaling, Front. Oncol. 10 (2020) 687.

[48] S.S. Dykes, C. Gao, W.K. Songock, R.L. Bigelow, G.V. Woude, J.M. Bodily, J.A. Cardelli, Zinc finger E-box binding homeobox-1 (Zeb1) drives anterograde lysosome trafficking and tumor cell invasion via upregulation of Na+/H+ Exchanger-1 (NHE1), Mol. Carcinog. 56 (2017) 722–734.

[49] S.R. Amith, J.M. Wilkinson, L. Fliegel, KR-33028, a potent inhibitor of the Na(+)/H(+) exchanger NHE1, suppresses metastatic potential of triple-negative breast cancer cells, Biochem. Pharmacol. 118 (2016) 31–39.

[50] T. Takatani-Nakase, C. Matsui, M. Hosotani, M. Omura, K. Takahashi, I. Nakase, Hypoxia enhances motility and EMT through the Na(+)/H(+) exchanger NHE-1 in MDA-MB-231 breast cancer cells, Exp. Cell. Res. 412 (2022) 113006.

[51] C.E.T. Donahue, M.D. Siroky, K.A. White, An optogenetic tool to raise intracellular pH in single cells and drive localized membrane dynamics, J. Am. Chem. Soc. 143 (2021) 18877–18887.